Interaction of two cylinders immersed in a viscous fluid. On the effect of moderate Keulegan–Carpenter numbers on the fluid forces

Maria Adela Puscas, Romain Lagrange

Interaction of two cylinders immersed in a viscous fluid. On the effect of moderate Keulegan-Carpenter numbers on the fluid forces.

Maria Adela Puscas[a], Romain Lagrange[b]

[a] *Université Paris-Saclay, CEA, Service de Thermo-hydraulique et de Mécanique des Fluides, F-91191, Gif-sur-Yvette, France*
[b] *Université Paris-Saclay, CEA, Service d'Etudes Mécaniques et Thermiques, F-91191, Gif-sur-Yvette, France*

Abstract

This work deals with the hydrodynamic interaction of two parallel circular cylinders, with identical radii, immersed in a viscous fluid initially at rest. One cylinder is stationary while the other one is imposed a harmonic motion with a moderate amplitude of vibration. The direction of motion is parallel to the line joining the centers of the two cylinders. The two dimensional fluid-structure problem is numerically handled by the Arbitrary Lagrangian-Eulerian method implemented in the open-source CFD code TrioCFD. First, we show that the fluid forces on the two cylinders are aligned with the direction of the imposed motion. Second, we show that the moderate oscillations of the moving cylinder create nonlinear effects in the fluid that strongly affect the characteristics (Fourier harmonics) of the hydrodynamic force acting on the stationary cylinder. The fluid force on the moving cylinder is shown to be poorly affected by the nonlinear effects, which makes it possible to extend the linear concept of self-added mass and damping coefficients. First, we show that the self-added coefficients decrease as $Sk^{-1/2}$, with Sk the Stokes number (dimensionless number constructed from the imposed vibration frequency). Second, we show that the self-added mass (resp. damping) decreases (resp. increases) as $-KC^3$ (resp. $+KC^3$), with KC the Keulegan-Carpenter number (ratio between the imposed amplitude vibration and the separation distance between the cylinders). These variations are included in new power laws derived from nonlinear regressions of the numerical results. These new power laws for the self-added coefficients combine the effect of both Sk and KC, covering the viscous ($Sk \geq 500$) and weakly nonlinear ($KC \leq 0.3$) regimes.

Keywords: Fluid-structure interaction; Keulegan-Carpenter number; Nonlinear effects; Stokes number; Viscous effects; Self-added coefficients; ALE method

1. Introduction

The analysis of forced vibrations of structures immersed in flowing or quiescent fluids is of fundamental importance in many scientific and engineering fields, spanning a wide range of applications, from the nuclear industry and the flow-induced vibrations of heat exchanger tubes [1, 2, 3], the dynamics of trees and plants [4], to the energy harvesting of flexible structures [5, 6, 7]. Since the seminal works of [8, 9, 10], a considerable amount of theoretical, numerical and experimental studies have been conducted, considering single or multiple immersed structures, rigid or flexible, with various geometries and kinematics (imposed or fluid coupled), and different fluid conditions or assumptions, see [11, 12, 13, 14, 15, 16] for an extensive review.

For small oscillations of an immersed body, the nonlinear convective acceleration of the Navier-Stokes equation is small compared with the unsteady acceleration, see [17]. The fluid forces are linear combinations of the velocity and the acceleration of the immersed body. The coefficients entering in these linear combinations are referred to as the added-mass term and the added-damping term. These coefficients are sensitive to the geometry of the moving body, the number of immersed structures, the degree of confinement of the problem, the viscosity of the fluid, and the characteristics of the motion (for e.g., the frequency of the motion, or in the case of a flexible structure the shape of its vibration modes, see [18]). In many practical cases, the Stokes number, defined as the ratio of the unsteady acceleration of the Navier-Stokes equations versus the viscous term, is large enough to consider the fluid forces to be purely inertial. In such cases, the added-damping coefficient is disregarded, whereas the added-mass coefficient can be obtained from a potential theory, solving the Laplace equation for a fluid potential, with given boundary conditions on the surface of the body and on the limits of the fluid domain. The reader is referred to the books of [19, 20] for a detailed presentation on the concept of the added-mass coefficient and the related calculation in different configurations.

In this paper, we consider the two dimensional problem of two circular cylinders immersed in a quiescent viscous fluid. One cylinder is stationary while the other is imposed a harmonic motion in the direction of the line connecting the center of the two cylinders. We expand on the findings of [17, 21] to explore the effect of

Email addresses: maria-adela.puscas@cea.fr (Maria Adela Puscas), romain.lagrange@cea.fr (Romain Lagrange)

finite amplitude vibrations on hydrodynamic loading. Specifically, we depart from small structural oscillations and linear fluid-structure interaction to consider finite-amplitude structural vibrations with Keulegan-Carpenter number up to 30%. The Keulegan-Carpenter number is defined as the ratio of the vibration amplitude versus the distance between the two cylinders and is used to measure the relative effect of convective acceleration with respect to local acceleration. Here, we consider Stokes numbers from 500 to 2000 and Keulegan-Carpenter numbers from 0.005 to 0.3. In this regime, viscous effects and convection-driven nonlinearities in the fluid-structure interaction are expected to be not negligible, as demonstrated in the literature on rigid cylinders in oscillatory flows, see [22, 23, 24], and recent works on vibrations of slender beams in unbounded viscous fluid, see [25, 26]. The fluid-structure problem is numerically handled by the Arbitrary Lagrangian-Eulerian (ALE) method [27] implemented in the open-source CFD code, TrioCFD, see [28, 29, 30].

The paper is organized as follows. § 2 presents the problem and the governing equations for two circular cylinders immersed in a viscous fluid initially at rest. The numerical approach used to solve the fluid-structure problem is briefly described in this section. § 3 presents the results of the numerical simulations for the fluid forces when one cylinder is stationary, and the other is imposed harmonic oscillations with different frequencies and increasing amplitudes. In § 4, nonlinear regressions of the numerical results are performed to extend the linear concept of self-added coefficients to the weakly nonlinear regime of moderate vibration amplitudes. Finally, some conclusions are drawn in § 5.

2. Definition of the problem and numerical approach

2.1. Presentation of the problem

We consider the two-dimensional problem of two parallel circular cylinders C_j, radius R, boundaries ∂C_j, immersed in a viscous stagnant fluid, characterized by its volume mass density ρ and its kinematic viscosity ν. The cylinders are separated by a distance E, as illustrated in Fig. 1. The cylinder C_1 remains stationary while C_2 is imposed a harmonic displacement $\mathbf{U} = Q\sin(\Omega\tau)\,\mathbf{e}_x$, with Q the amplitude, τ the time, Ω the angular frequency and $\mathbf{e}_x$ the direction of motion, parallel to the line joining the cylinder centers. The oscillations of C_2 generate an incompressible fluid flow ($\mathbf{V}$,P) governed by the Navier-Stokes equations

$$\nabla\cdot\mathbf{V} = 0, \tag{1a}$$

$$\frac{\partial\mathbf{V}}{\partial\tau} + (\mathbf{V}\cdot\nabla)\,\mathbf{V} + \frac{1}{\rho}\nabla P - \nu\Delta\mathbf{V} = \mathbf{0}, \tag{1b}$$

$$\mathbf{V} = \mathbf{0} \quad \text{on } \partial C_1, \tag{1c}$$

$$\mathbf{V} - \frac{d\mathbf{U}}{d\tau} = \mathbf{0} \quad \text{on } \partial C_2. \tag{1d}$$

The linear fluid force acting on C_j is the sum of a pressure and a viscous term and writes

$$\mathbf{F}_j = -\int_{\partial C_j} P\mathbf{n}dL + \rho\nu\int_{\partial C_j}\left[\nabla\mathbf{V} + (\nabla\mathbf{V})^T\right]\cdot\mathbf{n}dL, \tag{2}$$

with $\mathbf{n}$ the outward normal unit vector to ∂C_j, $(\nabla\mathbf{V})^T$ the transposate tensor of $\nabla\mathbf{V}$ and dL an infinitesimal line element of ∂C_j.

The dimensionless parameters of this study are

$$KC = \frac{Q}{E}, \quad Sk = \frac{R^2\Omega}{\nu}, \quad \varepsilon = \frac{E}{R}, \tag{3}$$

known as the Keulegan-Carpenter number, the Stokes number, and the dimensionless separation distance, respectively. In what follows, we note $t = \Omega\tau$ the dimensionless time, $\mathbf{f}_j = \mathbf{F}_j/\left(\rho Q R^2\Omega^2\right)$ the dimensionless fluid force and f_i its x-component.

2.2. Numerical approach

To solve Eq. (1), numerical simulations are performed with the open-source code TrioCFD, coupled with an Arbitrary Lagrangian-Eulerian (ALE) module. The reader is referred to [28, 29, 30, 27] for extensive details on the CFD code and the ALE module.

In the ALE approach, the fluid flow is computed in a domain that is deformed in order to follow the movement of the fluid-solid interface. The approach treats the mesh as a frame that moves with the arbitrary

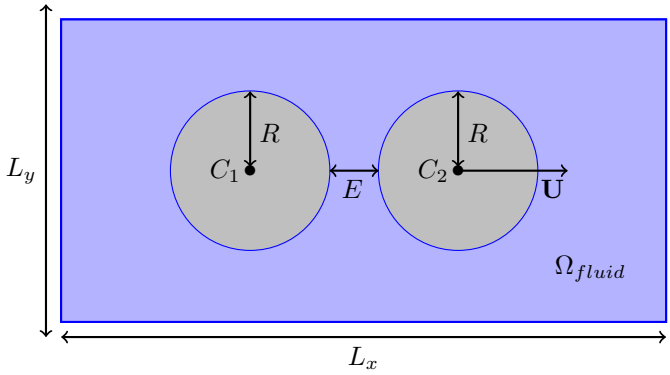

FIGURE 1 – Schematic diagram of two parallel circular cylinders with radius R, separated by a distance E, immersed in a viscous stagnant fluid domain Ω_{fluid}. The cylinder C_1 is fixed while C_2 is imposed a displacement vector $\mathbf{U}$.

velocity $\mathbf{V_{ALE}}$. For moderate deformations, $\mathbf{V}_{ALE}$ is usually defined as the solution of an auxiliary Laplace problem

$$\Delta \mathbf{V}_{ALE} = \mathbf{0}, \tag{4a}$$

$$\mathbf{V}_{ALE} = \mathbf{0} \quad \text{on } \partial\Omega_{fluid} \setminus \partial C_2 \ , \tag{4b}$$

$$\mathbf{V}_{ALE} - \frac{d\mathbf{U}}{d\tau} = \mathbf{0} \quad \text{on } \partial C_2. \tag{4c}$$

from which the kinematics of the mesh grid is updated. In this new frame of reference, the Navier-Stokes equation (1b) writes

$$\frac{\partial J\mathbf{V}}{\partial \tau} + J\left((\mathbf{V}\cdot\nabla)\,\mathbf{V} - (\mathbf{V_{ALE}}\cdot\nabla)\,\mathbf{V} + \frac{1}{\rho}\nabla P - \nu\Delta\mathbf{V} \right) = \mathbf{0}, \tag{5a}$$

with J the Jacobian of the transformation between the ALE and the Lagrange descriptions.

In our simulations, a first-order backward Euler scheme is used to time discretize the Navier-Stokes equations and the space discretization is based on the hybrid Finite Element-Volume method [29, 31] for unstructured grids, leading to the following discrete system

$$D\mathbf{V}_h^{n+1} = \mathbf{0}, \tag{6a}$$

$$M\frac{J^{n+1}\mathbf{V}_h^{n+1} - J^n\mathbf{V}_h^n}{\Delta t} - J^{n+1}\left(A\mathbf{V}_h^{n+1} - L(\mathbf{V}_h^n)\mathbf{V}_h^{n+1} + L(\mathbf{V}^n)\mathbf{V}_{h,ALE}^{n+1} - GP_h^{n+1} \right) = \mathbf{0}, \tag{6b}$$

where $\mathbf{V}_h$ is the discrete fluid velocity, P_h is the discrete fluid pressure, $\mathbf{V}_{h,ALE}$ the discrete mesh velocity, Δt the time step, M is the mass matrix, A is the discrete diffusion operator, $L(\mathbf{V}_h)$ is the non-linear discrete convection operator, G is the discrete gradient operator, and D is the discrete divergence operator. The superscripts n and $n+1$ indicate the time step at which the variable is computed. The nonlinear convective term, $L(\mathbf{V}_h^n)\mathbf{V}_h^{n+1}$, is approximate with the upwind MUSCL (Monotonic Upstream-centered Scheme for Conservation Laws, see [32]) scheme.

A projection-correction technique [33, 34] is employed to solve the velocity-pressure coupling. A predicted velocity $\mathbf{V}_h^*$ is computed

$$J^{n+1}\left(\frac{1}{\Delta t}M - A + L(\mathbf{V}_h^n) \right)\mathbf{V}_h^* = \frac{1}{\Delta t}MJ^n\mathbf{V}_h^n + J^{n+1}L(\mathbf{V}_h^n)\mathbf{V}_{h,ALE}^{n+1} - J^{n+1}GP_h^n, \tag{7}$$

and the mass conservation is then enforced by solving a Poisson equation for pressure

$$DM^{-1}G\left(P_h^{n+1} - P_h^n\right) = \frac{1}{\Delta t}D\mathbf{V}_h^*. \tag{8}$$

The velocity is corrected using the predicted velocity $\mathbf{V}_h^*$

$$\mathbf{V}_h^{n+1} = \mathbf{V}_h^* - \Delta t M^{-1}G\left(P_h^{n+1} - P_h^n\right). \tag{9}$$

Iterative solvers from the PETSc library (Portable, Extensible Toolkit for Scientific Computation, see [35]) solve the discrete equations (7) and (8).

3. Presentation of a case study

We now present the results of our two dimensional numerical simulations, considering the case in which the cylinder C_1 is fixed while C_2 is imposed a dimensionless displacement in the $\mathbf{e}_x$ direction, of the form $u = \sin(t)$. To investigate the weakly nonlinear effects generated by the oscillations of C_2 on the fluid forces, the Keulegan-Carpenter number is varied in the range $KC \in [0.005, 0.3]$. Four representative values were chosen for the Stokes number, $Sk \in \{500, 1000, 1500, 2000\}$, thereby covering a viscous regime for $Sk = 500$ and an almost inviscid regime for $Sk = 2000$. Finally, in all our numerical simulations, the dimensionless separation distance is $\varepsilon = 2$. Concerning the numerical setup, the fluid properties are $\nu = 1.007 \cdot 10^{-6}$ m^2/s, $\rho = 1000$ kg/m^3 and the two cylinders have the same radius, $R = 1$ m. The computational domain is rectangular and its size ($L_x = 11.5$ m and $L_y = 10.5$ m) is considered sufficiently large to minimize the end effects. To discretize the fluid domain, a locally refined grid of triangles generated by the open-source Gmsh mesh generator, see [36], is used. An analysis of mesh sensitivity yields convergent results with a mesh of 379610 triangles, see Table B.5 in Appendix B. This mesh refinement is used in all our numerical simulations.

3.1. Fluid forces

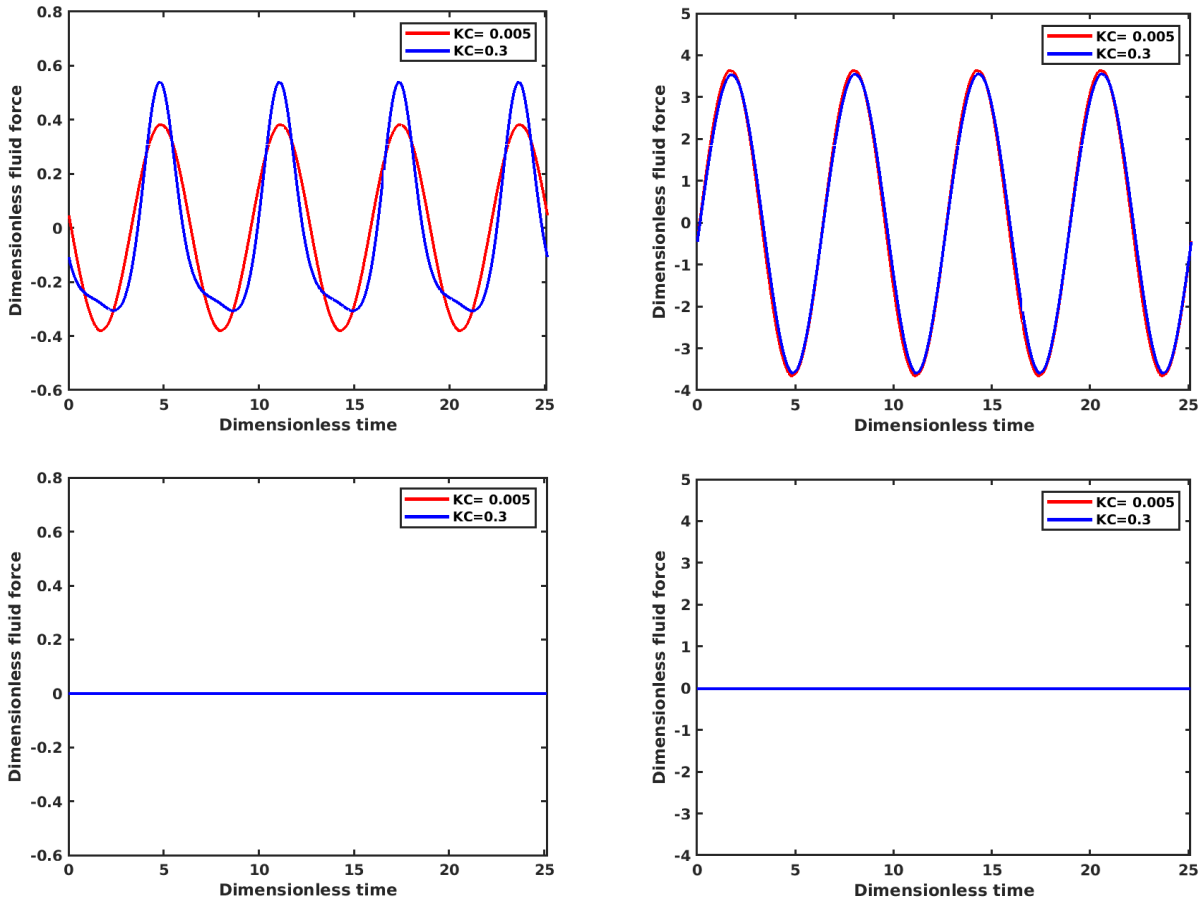

FIGURE 2 – Time evolution of the dimensionless fluid force, for two different values of the Keulegan-Carpenter number, $KC \in \{0.005, 0.3\}$. Top figures : x-component, f_i, of the fluid force. Bottom figures : y-component of the fluid force. On these figures the red ($KC = 0.005$) and blue ($KC = 0.3$) lines are superimposed. Left figure : fluid force acting on the fixed cylinder. Right figure : fluid force acting on the moving cylinder. The Stokes number is $Sk = 500$.

In Fig. 2, we show the time evolution of the x and y-components of the dimensionless fluid force $\mathbf{f}_i$, $i \in \{1, 2\}$, for $KC \in \{0.005, 0.3\}$ and $Sk = 500$. First, we observe that $\mathbf{f_i}$ has no component along the y-direction so that the fluid force $\mathbf{f}_i = f_i \mathbf{e}_x$ is aligned with the direction of motion of C_2. Second, we show that f_i is maximum on C_2, and is a periodic function whose amplitude, angle with respect to the imposed displacement, and more generally the overall shape, are affected by the value of the Keulegan-Carpenter number. For small values of KC, i.e. small vibration amplitudes of C_2, the magnitude of the convective term of the Navier-Stokes equations remains negligible. It follows that f_i is poorly affected by the nonlinear effects from the fluid and has a sinusoidal

shape, as the imposed displacement. For larger values of KC, such as $KC = 0.3$, the vibrations of C_2 create nonlinear effects in the fluid that strongly affect the shape of f_i (especially f_1).

To quantitatively determine the effects of KC on f_i, a nonlinear least-squares formulation is used to fit a model to numerical data. As f_i is a periodic function, a Fourier model of the form

$$f_i(t) = \frac{a_0}{2} + \sum_{j=1}^{N} \left[a_j \cos\left(j\omega t\right) + b_j \sin\left(j\omega t\right)\right] = \frac{a_0}{2} + \sum_{j=1}^{N} h_j \sin\left(j\omega t + \phi_j\right), \tag{10}$$

is used with $\{a_j, b_j, \omega\}$ a set of $2(N+1)$ fitting parameters. These fitting parameters, namely the real Fourier coefficients a_j, b_j and the angular frequency ω, are functions of the dimensionless separation distance, ε, the Stokes number, Sk, and the Keulegan-Carpenter number, KC. The magnitude h_j and the phase ϕ_j of the j-th Fourier harmonics of f_i, see second equality of (10), are defined as $h_j = \sqrt{a_j^2 + b_j^2}$ and $\phi_j = \arg\left(b_j + \mathrm{i}a_j\right)$. With such a definition of ϕ_j, the j-th Fourier harmonics of f_i is in phase (resp. in phase opposition) with the imposed displacement if $\phi_j = 0$ (resp. $\phi_j = \pi$). From the fitting parameters $\{a_j, b_j\}$, we also define

$$THD = 1 - \frac{a_1^2 + b_1^2}{\sum_{j=1}^{N}\left(a_j^2 + b_j^2\right)}, \qquad M = \frac{a_0}{2}, \qquad A = \sqrt{\frac{a_0^2}{4} + \frac{1}{2}\sum_{j=1}^{N}\left(a_j^2 + b_j^2\right)}, \tag{11}$$

as the total harmonic distorsion, the mean value, and the Root Mean Square (RMS) amplitude of f_i, respectively. The total harmonic distorsion is an indicator of the importance of the nonlinear effects present in the fluid force signal f_i. The root mean square amplitude A indicates the deviation of f_i from its mean value $a_0/2$. Finally, we note A_0 and ω_0 the limit of A and ω, respectively, as $KC \to 0$.

3.2. Effect of the Keulegan-Carpenter number

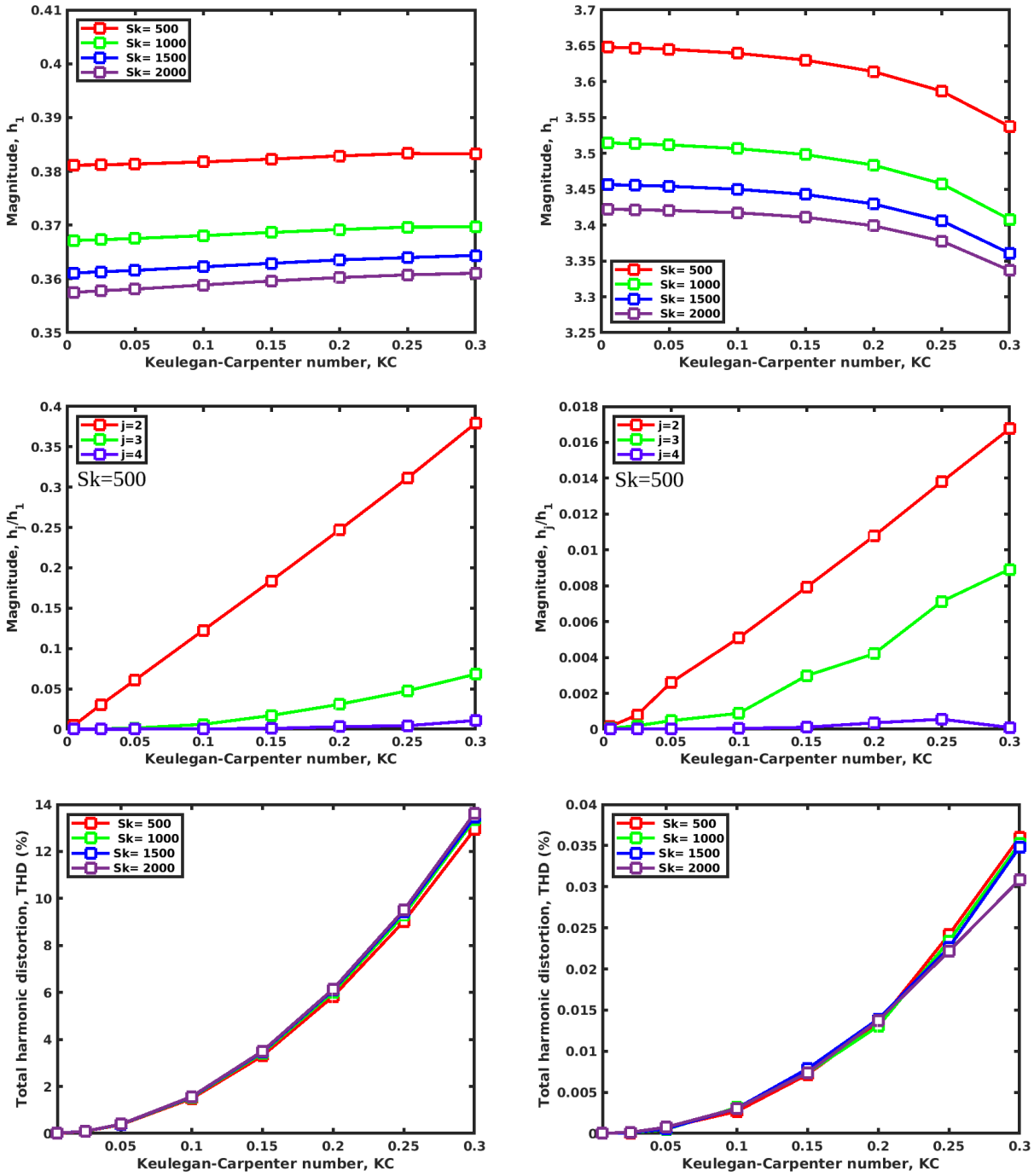

FIGURE 3 – Evolution of the magnitude, h_1 of the fundamental harmonic of the fluid force, the normalized magnitude, h_j/h_1 of the j-th harmonic, and the total harmonic distortion, THD, as a function of the Keulegan-Carpenter number, KC, for different values of the Stokes number, $Sk \in \{500, 1000, 1500, 2000\}$. Left figure : fluid force f_1 acting on the fixed cylinder. Right figure : fluid force f_2 acting on the moving cylinder.

In Fig. 3, we show that the magnitude of all the harmonics of the fluid force f_i, $i \in \{1, 2\}$, decreases as the Stokes number Sk increases. Thus f_i is all the more intense as the viscous effects are important, as already observed by [21] in the case of small oscillations of C_2, i.e. $KC \to 0$. For moderate oscillations of C_2, the magnitude of all the harmonics of f_1 also increases as the Keulegan-Carpenter number KC increases. For $KC = 0.3$, we observe that the magnitude of the second harmonic of f_1 is about 37% of the magnitude of the fundamental harmonic, thus explaining the nonlinear effects shown in the time evolution of f_1, depicted in Fig. 2. As expected, the strengthening of all the harmonics of f_1 as KC increases eventually yields an increase of its total harmonics distortion. On the other side, the magnitude of the fundamental harmonic (resp. sub-

harmonics) of f_2 decreases (resp. increases) as KC increases. This behavior indicates that the kinetic energy of C_2 is transferred to the fluid, and distributed from the fundamental harmonic of the pressure field to the sub-harmonics. For $KC \leq 0.3$, the magnitude of the sub-harmonics of f_2 remains very small compared to the magnitude of the fundamental harmonic. Still, this effect is sufficiently sensitive to generate a slight increase of the total harmonic distortion of f_2 as KC increases. Finally, the variations of h_j shown in Fig. 3 confirm that the moderate oscillations of C_2 create some nonlinear effects in the fluid that tend to intensify (resp. weaken) the hydrodynamic force acting on the stationary (resp. moving) cylinder, as expected from the observation of the time signals in Fig. 2.

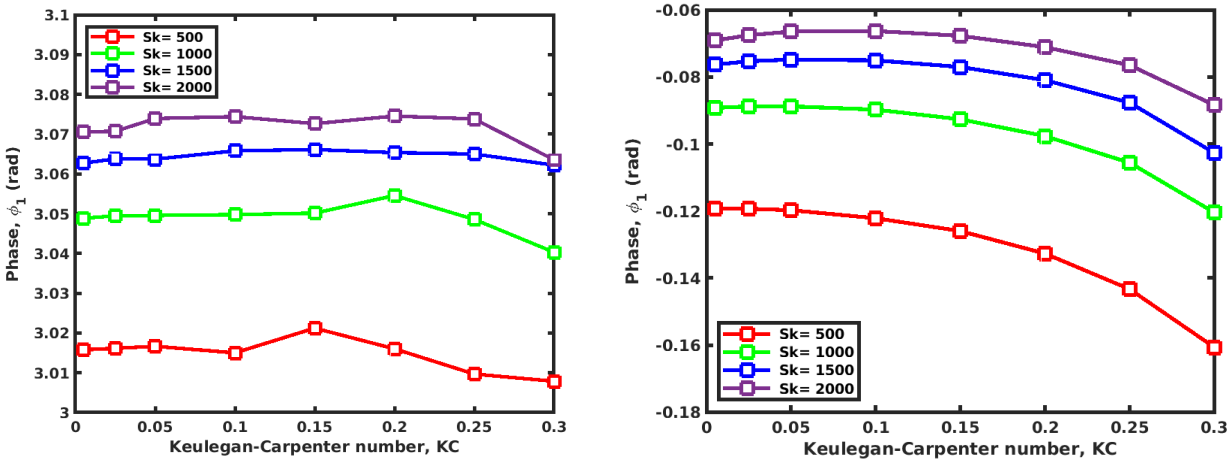

FIGURE 4 – Phase, ϕ_1 of the fundamental harmonic of the fluid force, as a function of the Keulegan-Carpenter number, KC, for different values of the Stokes number, $Sk \in \{500, 1000, 1500, 2000\}$. Left figure : fluid force f_1 acting on the fixed cylinder. Right figure : fluid force f_2 acting on the moving cylinder.

Having analyzed the variations of the magnitude of the harmonics of f_i, we now proceed with the discussion on the variations of the phase ϕ_1 of the fundamental harmonic of f_i. In Fig. 4 we show that the two forces have fundamental harmonics that are nearly in phase opposition, as expected from the time evolutions of the fluid forces shown in Fig. 2. At first order, the fundamental harmonic of f_1 (resp. f_2) is in phase opposition (resp. in phase) with the imposed sinusoidal displacement of C_2. The phase of the fundamental harmonic of f_i, $i \in \{1, 2\}$, is sensitive to the Stokes number and is shown to increase as Sk decreases, as already observed by [21] in the case of small oscillations of C_2, i.e. $KC \to 0$. For moderate oscillations of C_2, the phase of the fundamental harmonic of f_1 is poorly sensitive to the Keulegan-Carpenter number whereas the phase of the fundamental harmonic of f_2 exhibits a slight decrease as KC increases. The variations of ϕ_j with the Stokes and the Keulegan-Carpenter numbers imply that the direction of the fluid force f_i depends on both Sk and KC. For one oscillation of the moving cylinder C_2, the fluid force f_i vanishes and reverses its direction when $f_i(t) = 0$, i.e. when $t = t_i^{(1)}$ and $t = t_i^{(2)}$. At these two specific times, the dimensionless displacement of the moving cylinder is $u_i^{(1)} = \sin\left(t_i^{(1)}\right)$ and $u_i^{(2)} = \sin\left(t_i^{(2)}\right) > u_i^{(1)}$. In Fig. 5, we show that f_1 is positive (resp. negative) when $-1 \leq u \leq u_1^{(1)}$ (resp. $u_1^{(2)} \leq u \leq 1$). As f_2 is at first order in phase opposition with f_1, it is negative (resp. positive) when $-1 \leq u \leq u_2^{(1)}$ (resp. $u_2^{(2)} \leq u \leq 1$). It follows that the fluid forces cause the cylinders to attract (resp. repel) each other when $-1 \leq u \leq \min\left(u_1^{(1)}, u_2^{(1)}\right)$ (resp. $\max\left(u_1^{(2)}, u_2^{(2)}\right) \leq u \leq 1$). In the narrow range $u_i^{(1)} \leq u \leq u_i^{(2)}$ the sign of f_i depends on the direction of motion of the cylinder C_2. When C_2 approaches C_1, f_1 (resp. f_2) is negative (resp. positive) so that the fluid forces cause the cylinders to repel each other when $\max\left(u_1^{(1)}, u_2^{(1)}\right) \leq u \leq \min\left(u_1^{(2)}, u_2^{(2)}\right)$. On the contrary, when C_2 moves away from C_1, f_1 (resp. f_2) is positive (resp. negative). In that case, the fluid forces cause the cylinders to attract each other when $\max\left(u_1^{(1)}, u_2^{(1)}\right) \leq u \leq \min\left(u_1^{(2)}, u_2^{(2)}\right)$.

To assess the validity of our numerical predictions, we refer to the work of [10] who considered the small oscillations, i.e. $KC \to 0$, of an isolated cylinder, i.e. $\varepsilon \to \infty$, immersed in a viscous fluid initially at rest. In such a case the fluid problem is fully linear and can be solved by introducing a stream-function from which the fluid force $f_2(t) = \Re\{e^{it}\bar{f}_2\}$ is derived, $\Re$ being the real part operator. For a harmonic displacement, i.e.

$u(t) = \Re\{e^{it}\bar{u}\}$, the complex representation of the force writes

$$\bar{f}_2 = \bar{u}\pi \left[1 + \frac{4}{\sqrt{\mathrm{i}Sk}} \frac{\mathrm{K}_1\left(\sqrt{\mathrm{i}Sk}\right)}{\mathrm{K}_0\left(\sqrt{\mathrm{i}Sk}\right)} \right], \tag{12}$$

with K_0 and K_1 the modified Bessel functions of second kind. The change of sign of the fluid force function occurs when $t = -\arg\left(\bar{f}_2/\bar{u}\right) + k\pi$, $k \in \mathbb{Z}$, leading to

$$u_2^{(j)} = (-1)^j \left| \sin\left(\arg\left(\bar{f}_2/\bar{u}\right)\right) \right|. \tag{13}$$

In Fig. 5 , we show that the graph of Eq. (13) is in line with the one obtained numerically for $KC = 0.005$, thereby corroborating our predictions.

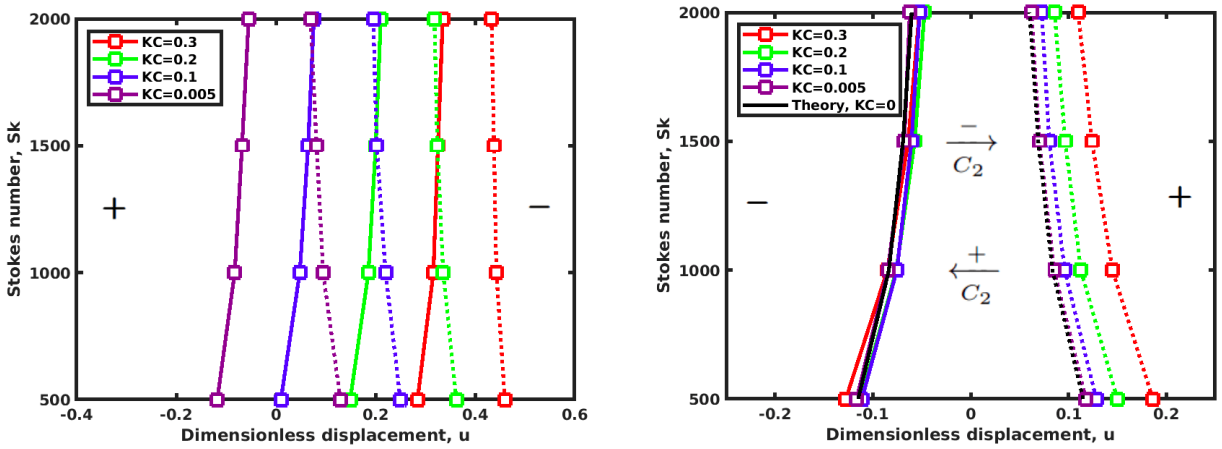

FIGURE 5 – Direction ($+\mathbf{e}_x$ or $-\mathbf{e}_x$) of the fluid forces, depending on $Sk \in \{500, 1000, 1500, 2000\}$, $KC \in \{0.005, 0.1, 0.2, 0.3\}$ and the dimensionless displacement u of C_2. Left figure : fluid force f_1 acting on the fixed cylinder. Right figure : fluid force f_2 acting on the moving cylinder. On this figure the arrows show the direction of motion of C_2. The black line shows the graph of Eq. (13), derived in the case of an isolated cylinder with $KC \to 0$. In both figures, the open symbols represent numerical results. The solid (resp. dashed) lines correspond to $u = u_i^{(1)}$ (resp. $u = u_i^{(2)}$). .

Having analyzed the properties of the Fourier harmonics of the fluid forces, we now proceed with the determination of the variations of the angular frequency ω, mean value M and RMS amplitude A of f_i, as KC and Sk are varied. The quantities ω_0, $M_0 = 0$ and A_0, corresponding to $KC \to 0$, are used as references. In Fig. 6, we show the variations of ω/ω_0, M and A/A_0 for $KC \leq 0.3$. For all Stokes numbers $Sk \in \{500, 1000, 1500, 2000\}$, we observe that ω/ω_0 is a constant function of KC. It follows that the moderate oscillations of C_2 do not significantly affect the period of f_i, so that $\omega = \omega_0 = 2\pi$. These moderate vibration amplitudes mostly affect the dimensionless mean value M and the RMS amplitude ratio A/A_0 of f_i. The mean value of f_1 (resp. f_2) is shown to linearly decrease (resp. increase) as KC increases. On the other hand, the RMS amplitude ratio of f_1 (resp. f_2) increases as KC^2 (resp. decrease as $-KC^3$) as KC increases.

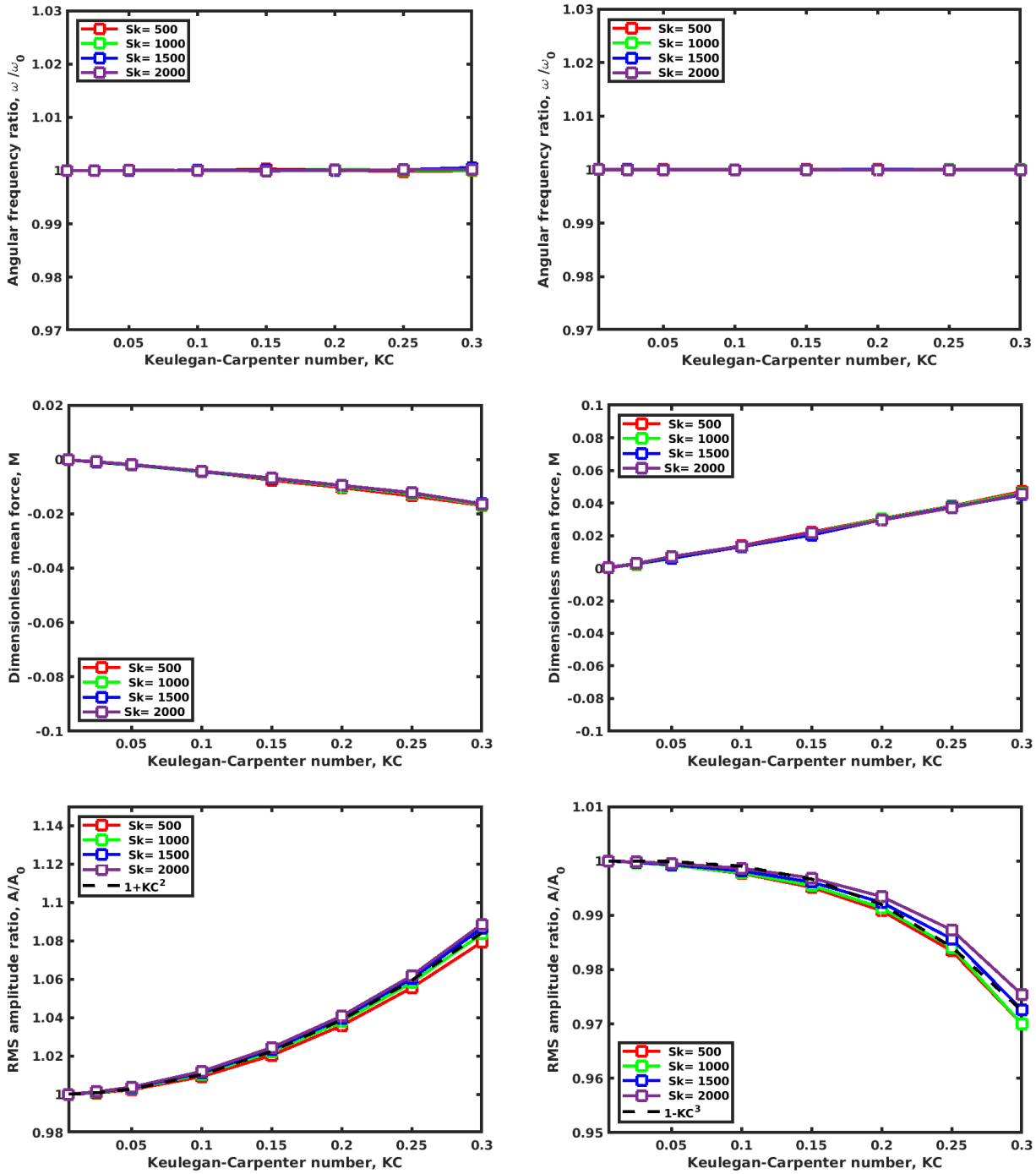

FIGURE 6 – Evolution of the angular frequency ratio, ω/ω_0, dimensionless mean value, M, and RMS amplitude ratio A/A_0 of the dimensionless fluid force f_i, as a function of the Keulegan-Carpenter number, KC, for different values of the Stokes number, $Sk \in \{500, 1000, 1500, 2000\}$. Left figures : fluid force f_1 acting on the fixed cylinder. Right figures : fluid force f_2 acting on the moving cylinder.

4. Self-added coefficients and power laws

In the previous section, we have shown that the amplitude of the sub-harmonics of f_2 remain small compared with the amplitude of the fundamental harmonic, and that even in the case of moderate vibration amplitudes of C_2. Thus, in first approximation, f_2 is a linear combination of $\cos(t)$ and $\sin(t)$. Introducing $m_{self} = b_1/\pi$ and $c_{self} = -a_1/\pi$ as the self-added mass and damping coefficients, see [21], f_2 writes

$$f_2(t) \approx \pi \left[m_{self} \sin(t) - c_{self} \cos(t) \right]. \tag{14}$$

The self-added coefficients relate the fluid force acting on the cylinder C_2 due to its own motion. As a_1 and b_1, these coefficients depend on both the Keulegan-Carpenter number, the Stokes number and the dimensionless

separation distance. As shown in § 3.2, the fluid force on C_1 is affected by the nonlinear effects and so does not express as a linear combination between the velocity of C_2 and its acceleration. Therefore, the linear concept of cross-added mass and damping coefficients cannot be extended to the case of moderate oscillations of C_2.

In Fig. 7, we show that $m_{self} \to m_0$ as $KC \to 0$ and decreases monotonically as KC increases in the range $[0, 0.3]$. The self-added damping coefficient first slightly decreases from its asymptotic limit $c_{self} \to c_0$ as $KC \to 0$, and eventually increases as KC increases. From these variations and in first approximation, it is assumed that the fluid added-coefficients follow power laws of the form $m_{self} = m_0\,(1 + m_1 Sk^{q_m} KC^{p_m})$ and $c_{self} = c_0\,(1 + c_1 Sk^{q_c} KC^{p_c})$, with m_0, c_0 some functions of (Sk, ε) and m_1, c_1 some functions of ε only. The self-similarity of the lines in Fig. 7, obtained for different Stokes numbers $Sk \in \{500, 1000, 1500, 2000\}$, also suggests that p_m and p_c do not depend on Sk. In our analysis, we assume that q_m, p_m, q_c and p_c actually do not depend on ε, and therefore are constant power coefficients.

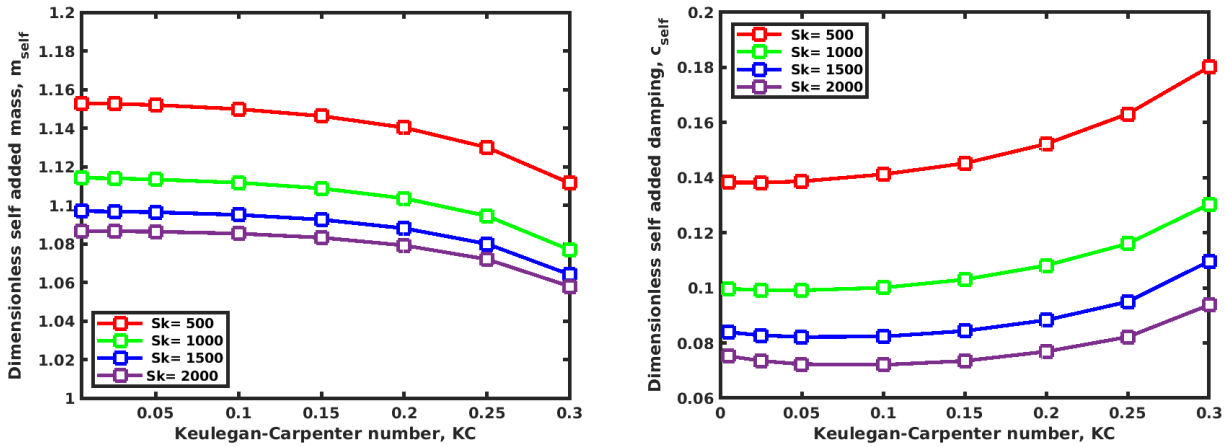

FIGURE 7 – Evolution of the dimensionless self-added coefficients, m_{self} and c_{self}, as a function of the Keulegan-Carpenter number, KC.

To precisely determine these constants, we first study the variations of m_0 and c_0 with the Stokes number, by carrying out numerical simulations for small vibrations amplitudes of C_2, i.e. $KC = 0.005$. The evolutions of m_0 and c_0 are depicted in Fig. 8, for $Sk \in [100, 900]$. In agreement with the theoretical predictions of [21], we show that m_0 and c_0 decreases as $Sk^{-1/2}$. Noting m_{00} the limit of m_{self} as $Sk \to \infty$ (inviscid limit, i.e. $c_{00} = 0$), we assume that m_0 and c_0 follow power laws of the form

$$m_0 \approx m_{00}\,(\varepsilon)\left(1 + \frac{m_{01}\,(\varepsilon)}{Sk^{1/2}}\right), \qquad c_0 \approx \frac{c_{01}\,(\varepsilon)}{Sk^{1/2}}, \tag{15}$$

with m_{00}, m_{01} and c_{01}, some functions of ε.

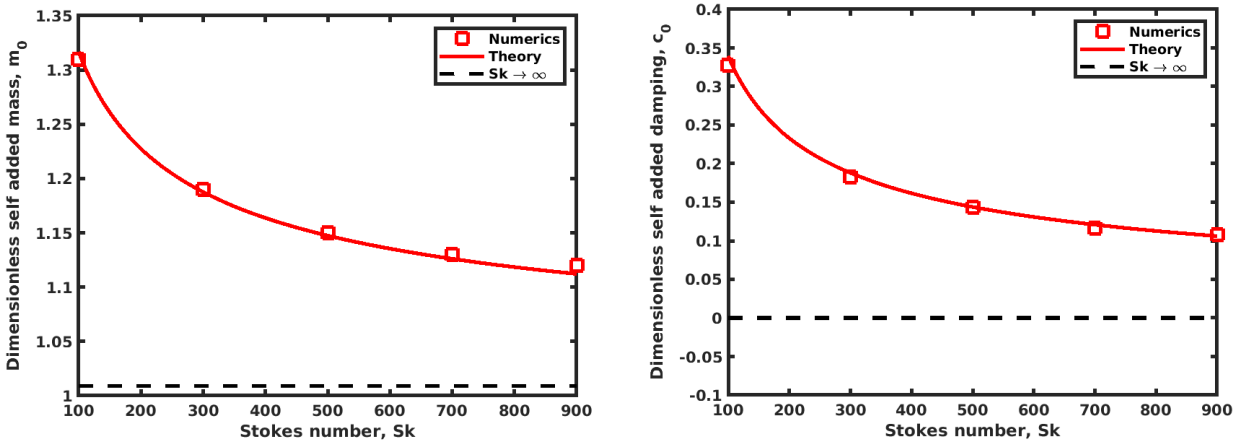

FIGURE 8 – Evolution of the dimensionless self-added coefficients, m_0 and c_0, as a function of the Stokes number, Sk. The solid lines are theoretical predictions from [21] and the open symbols are numerical results. The horizontal dashed lines correspond to the asymptotic limits $Sk \to +\infty$. The Keulegan-Carpenter number is $KC = 0.005$.

Having obtained power laws for the small oscillation terms, m_0 and c_0, a nonlinear least-squares formulation is used to fit the numerical data shown in Fig. 7 (and given in Appendix A) to the models for moderate oscillations, i.e. $m_{self} = m_0\left(1 + m_1 Sk^{q_m} KC^{p_m}\right)$ and $c_{self} = c_0\left(1 + c_1 Sk^{q_c} KC^{p_c}\right)$. This formulation yields power constants $q_m = -1/4$, $p_m = 3$, $q_c = 1/8$ and $p_c = 3$ so that the added-mass and damping coefficients eventually write

$$m_{self} \approx m_{00}(\varepsilon)\left(1 + \frac{m_{01}(\varepsilon)}{Sk^{1/2}}\right)\left(1 + \frac{m_1(\varepsilon)}{Sk^{1/4}} KC^3\right), \qquad c_{self} \approx \frac{c_{01}(\varepsilon)}{Sk^{1/2}}\left(1 + c_1(\varepsilon)\, Sk^{1/8} KC^3\right), \tag{16}$$

with m_1 and c_1 some functions of ε. For $\varepsilon = 2$, the nonlinear least-squares formulation yields $m_{00} = 1.009$, $m_{01} = 2.8$, $m_1 = -6.5$, $c_{01} = 3.14$ and $c_1 = 4.81$. In Fig. 9, we show that the predictions from the power laws (16) are in very good agreement with the numerical results, and that for all the Stokes and Keulegan-Carpenter numbers simulated. Indeed, the relative deviation δ between the numerical results and the predictions from the power laws is less than 0.25% for the self-added mass coefficient and less than 7% for the self-added damping coefficient, see Tables A.1-A.4 in Appendix A.

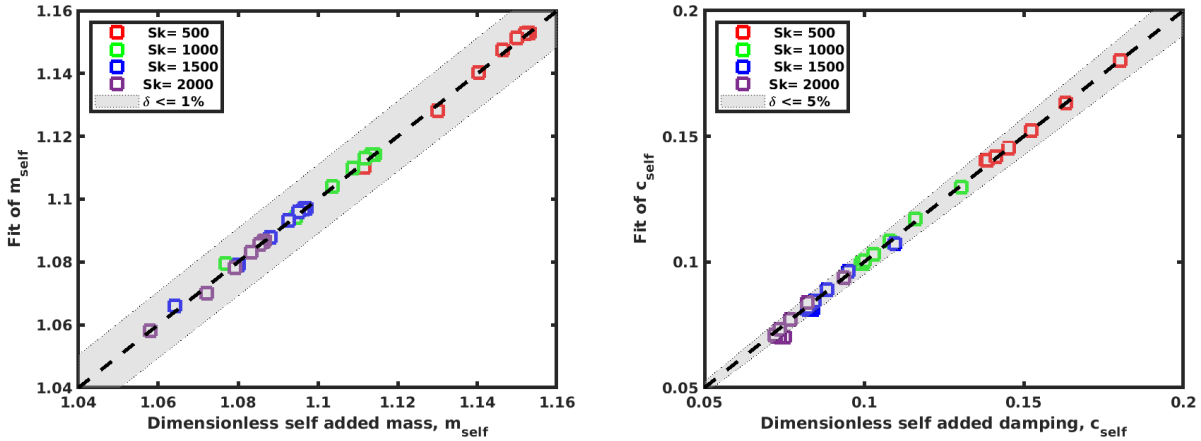

FIGURE 9 – Comparison between the dimensionless self-added coefficients, m_{self} and c_{self}, obtained numerically, and those predicted by the fitted power laws (16). The shaded gray areas show the relative deviations $\delta \leq 1\%$ and $\delta \leq 5\%$. The dashed lines correspond to $\delta = 0\%$.

The power laws (16) have been obtained for $Sk \geq 500$ and in the limit of moderate Keulegan-Carpenter numbers, $KC \leq 0.3$. These new laws extend the concept of the self-added coefficients, initially introduced for linear problems involving small oscillations of an immersed structure, to the case of weakly nonlinear problems involving moderate oscillations.

5. Conclusion

In the present work, we have considered the interaction of two parallel circular cylinders immersed in a fluid at rest. Two dimensional numerical simulations have been performed to determine the fluid forces acting on the cylinders when one of them is imposed a harmonic motion with moderate vibration amplitudes.The direction of the imposed motion is parallel to the line joining the cylinder centers. First, we showed that the fluid forces on the two cylinders have only one component, along the direction of motion. Second, we showed that moderate vibration amplitudes enhanced nonlinear effects in the fluid, leading to increasing sub-harmonic Fourier components in the time signal of the fluid force acting on the stationary cylinder. The force on the moving cylinder has a strong fundamental harmonic, negligible sub-harmonics, so that it is poorly affected by the fluid nonlinear effects. From this observation, we have extended the concept of the self-added coefficients, initially introduced for linear problems involving small oscillations of the cylinder, to the case of weakly nonlinear problems involving moderate oscillations. Nonlinear regressions of our numerical results yielded new power laws for the self added-coefficients, expressed in terms of the Stokes and the Keulegan-Carpenter numbers. We showed that the two coefficients scale as $Sk^{-1/2}$, whereas the self-added mass (resp. damping) decreases (resp. increases) as $-KC^3$ (resp. $+KC^3$).

In future work, we will perform numerical simulations considering various values of the dimensionless separation distance, in order to derive new laws for the functions of ε appearing in (16). We will then investigate the highly viscous regimes, i.e. $Sk \ll 500$, which require adequate meshes to accurately reproduce the fluid flow in the boundary layer of the moving cylinder. Finally, we shall investigate the case of large oscillations, i.e. $KC \gg 0.3$, to reveal the limitations of the linear concept associated to the self-added coefficients.

Appendix A. Tables of results

In this appendix, we provide the numerical and fitted values, see Eq. (16), of the self-added coefficients, depicted in Fig. A.10. These values are reported in Table A.1 for $Sk = 500$, A.2 for $Sk = 1000$, A.3 for $Sk = 1500$, and Table A.4 for $Sk = 2000$.

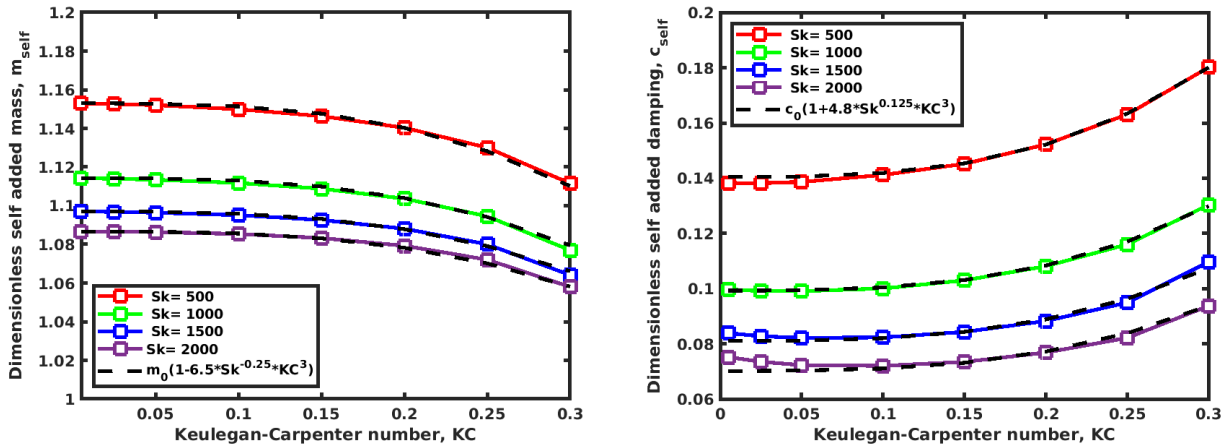

Figure A.10 – Evolution of the dimensionless self-added coefficients, m_{self} and c_{self}, as a function of the Keulegan-Carpenter number, KC. Open circles are numerical results. The black dashed lines are the graphs of the fitted power laws (16).

KC	Numerics TrioCFD		Fitted power laws		Relative deviation (%)	
	m_{self}	c_{self}	m_{self}	c_{self}	m_{self}	c_{self}
0.005	1.1529	0.1383	1.1529	0.1404	0	1.5459
0.025	1.1526	0.1382	1.1529	0.1404	0.0260	1.6198
0.05	1.1520	0.1386	1.1527	0.1406	0.0642	1.4084
0.1	1.1499	0.1412	1.1514	0.1419	0.1279	0.5003
0.15	1.1463	0.1452	1.1476	0.1454	0.1108	0.1218
0.2	1.1403	0.1522	1.1403	0.1522	0.0028	0.0367
0.25	1.1300	0.1631	1.1282	0.1634	0.1597	0.1717
0.3	1.1115	0.1802	1.1102	0.1801	0.1178	0.0356

Table A.1 – Comparison between the numerical results and the fitted power laws (16) for the dimensionless self-added coefficients. The maximum relative deviation is highlighted in red color. The Stokes number is $Sk = 500$.

KC	Numerics TrioCFD		Fitted power laws		Relative deviation (%)	
	m_{self}	c_{self}	m_{self}	c_{self}	m_{self}	c_{self}
0.005	1.1143	0.0997	1.1143	0.0993	0	0.3987
0.025	1.1139	0.0992	1.1142	0.0993	0.0267	0.1498
0.05	1.1134	0.0991	1.1141	0.0994	0.0612	0.3325
0.1	1.1117	0.1001	1.1130	0.1004	0.1114	0.3693
0.15	1.1088	0.1030	1.1099	0.1031	0.1015	0.1049
0.2	1.1036	0.1081	1.1040	0.10842	0.0296	0.2123
0.25	1.0945	0.1160	1.0941	0.1170	0.0331	0.8416
0.3	1.0769	0.1304	1.0795	0.1299	0.2274	0.3564

Table A.2 – Comparison between the numerical results and the fitted power laws (16) for the dimensionless self-added coefficients. The maximum relative deviation is highlighted in red color. The Stokes number is $Sk = 1000$.

KC	Numerics TrioCFD		Fitted power laws		Relative deviation (%)	
	m_{self}	c_{self}	m_{self}	c_{self}	m_{self}	c_{self}
0.005	1.0970	0.0839	1.0970	0.0811	0	3.3651
0.025	1.0968	0.0828	1.0970	0.0811	0.0191	2.0319
0.05	1.0964	0.0822	1.0969	0.0812	0.0436	1.1914
0.1	1.0951	0.0823	1.0959	0.0820	0.0729	0.3622
0.15	1.0926	0.0843	1.0931	0.0844	0.0509	0.0211
0.2	1.0881	0.0883	1.0878	0.0889	0.0212	0.6583
0.25	1.0800	0.0950	1.0791	0.0963	0.0828	1.4013
0.3	1.0641	0.1096	1.0661	0.1074	0.1796	2.0887

Table A.3 – Comparison between the numerical results and the fitted power laws (16) for the dimensionless self-added coefficients. The maximum relative deviation is highlighted in red color. The Stokes number is $Sk = 1500$.

KC	Numerics TrioCFD		Fitted power laws		Relative deviation (%)	
	m_{self}	c_{self}	m_{self}	c_{self}	m_{self}	c_{self}
0.005	1.0867	0.0752	1.0867	0.0702	0	6.6559
0.025	1.0866	0.0735	1.0866	0.0702	0.0064	4.4836
0.05	1.0863	0.0723	1.0865	0.0703	0.0173	2.7282
0.1	1.0853	0.0721	1.0856	0.0711	0.0243	1.3541
0.15	1.0833	0.0735	1.0831	0.0732	0.0147	0.4382
0.2	1.0792	0.0769	1.0782	0.0772	0.0940	0.4347
0.25	1.0720	0.0822	1.0702	0.0839	0.1738	2.0658
0.3	1.0580	0.0938	1.0581	0.0938	0.0139	0.0288

Table A.4 – Comparison between the numerical results and the fitted power laws (16) for the dimensionless self-added coefficients. The maximum relative deviation is highlighted in red color. The Stokes number is $Sk = 2000$.

Appendix B. Mesh convergence

In this appendix, we present the results of a mesh sensitivity analysis conducted for $Sk = 900$, $KC = 0.005$ and a dimensionless separation distance $\varepsilon = 2$. The Table B.5 shows that the two dimensional mesh with 379610 triangles is sufficiently refined to accurately estimate the self-added coefficients. This mesh uses two different local sizes for the elements: a small local size of 0.02 m for the elements close to the cylinders, and a large global size of 0.08 m for the other elements.

	m_0	c_0
Theoretical predictions of [21]	1.11	0.105
Dimension of the mesh	Numerics	Numerics
29620	1.09	0.134
110116	1.11	0.112
242916	1.12	0.108
379610	1.12	0.106
678 088	1.12	0.106

Table B.5 – Mesh convergence. The Stokes number is $Sk = 900$ and the Keulegan-Carpenter number is $KC = 0.005$.

References

[1] S. S. Chen, Vibration of nuclear fuel bundles, Nuclear Engineering and Design. 35 (1975) 399–422.

[2] S. S. Chen, Dynamics of heat exchanger tube banks, Journal of Fluids Engineering. 99 (1977) 462–469.

[3] F. Axisa, J. Antunes, B. Villard, Random excitation of heat exchangertubes by cross-flows, Journal of fluids and structures 4 (3) (1990) 321–341.

[4] E. de Langre, Effects of wind on plants, Annual Review of Fluid Mechanics 40 (1) (2008) 141–168.

[5] S. Michelin, O. Doare, Energy harvesting efficiency of piezoelectric flags in axial flows, Journal of Fluid Mechanics. 714 (2013) 489–504.

[6] E. Virot, X. Amandolese, P. Hemon, Coupling between a flag and a spring-mass oscillator, Journal of Fluids and Structures. 65 (2016) 447–454.

[7] C. Eloy, R. Lagrange, C. Souilliez, L. Schouveiler, Aeroelastic instability of cantilevered flexible plates in uniform flow, Journal of Fluid Mechanics. 611 (2008) 97–106.

[8] S. D. Poisson, Sur les mouvements simultanés d'un pendule et de l'air environnant, Mem. Acad. Roy. Sc., 1832.

[9] G. Green, Researches on the vibration of pendulums in fluid media, Transactions of the Royal Society of Edinburgh. 13 (1833) 54–68.

[10] G. G. Stokes, On some cases of fluid motion, Mathematical and Physical Papers. (2009) 17–68.

[11] S. S. Chen, Flow-induced vibration of circular cylindrical structures, Hemisphere Pub. Corp, 1987.

[12] R. D. Blevins, Flow-induced vibration, 2nd Edition, Krieger Publishing Company, 1990.

[13] M. P. Paidoussis, S. J. Price, E. de Langre, Fluid-Structure Interactions: Cross-Flow-Induced Instabilities, Cambridge University Press, 2010.

[14] T. Nakamura, S. Kaneko, F. Inada, M. Kato, K. Ishihara, T. Nishihara, N. W. Mureithi, M. A. Langthjem, Flow-induced vibrations: classifications and lessons from practical experiences, Butterworth-Heinemann, 2013.

[15] Y. Bazilevs, K. Takizawa, T. E. Tezduyar, Computational fluid-structure interaction: methods and applications, John Wiley & Sons, 2013.

[16] J.-F. Sigrist, Fluid-structure interaction: an introduction to finite element coupling, John Wiley & Sons, 2015.

[17] R. Lagrange, X. Delaune, P. Piteau, L. Borsoi, J. Antunes, A new analytical approach for modeling the added mass and hydrodynamic interaction of two cylinders subjected to large motions in a potential stagnant fluid, Journal of Fluids and Structures. 77 (2018) 102–114.

[18] R. Lagrange, M. A. Puscas, Hydrodynamic interaction between two flexible finite length coaxial cylinders: new theoretical formulation and numerical validation, Journal of Applied Mechanics, 89 (8) (2022) 081006.

[19] K. T. Patton, Tables of hydrodynamic mass factors for translational motion, The American Society of Mechanical Engineers, 1965.

[20] A. Korotkin, Added Masses of Ship Structures, Vol. 88, 2009. doi:10.1007/978-1-4020-9432-3.

[21] R. Lagrange, Y. Fraigneau, New estimations of the added mass and damping of two cylinders vibrating in a viscous fluid, from theoretical and numerical approaches, Journal of Fluids and Structures. 92 (2020) 102818.

[22] R. D. Gabbai, H. Benaroya, An overview of modeling and experiments of vortex-induced vibration of circular cylinders, Journal of sound and vibration 282 (3-5) (2005) 575–616.

[23] T. Sarpkaya, Force on a circular cylinder in viscous oscillatory flow at low Keulegan–Carpenter numbers, Journal of Fluid Mechanics 165 (1986) 61–71.

[24] T. Sarpkaya, Hydrodynamic damping, flow-induced oscillations, and biharmonic response, Journal of offshore Mechanics and Arctic engineering 117 (4) (1995).

[25] M. Aureli, M. Porfiri, Low frequency and large amplitude oscillations of cantilevers in viscous fluids, Applied Physics Letters 96 (16) (2010) 164102.

[26] M. Aureli, M. Basaran, M. Porfiri, Nonlinear finite amplitude vibrations of sharp-edged beams in viscous fluids, Journal of sound and vibration 331 (7) (2012) 1624–1654.

[27] J. Donea, A. Huerta, J. P. Ponthot, A. Rodríguez-Ferran, Arbitrary Lagrangian–Eulerian Methods, American Cancer Society, 2004.

[28] P. E. Angeli, U. Bieder, G. Fauchet, Overview of the TrioCFD code: Main features, V&V procedures and typical applications to nuclear engineering, in: Proceedings of 16th International Topical Meeting on Nuclear Reactor Thermal Hydraulics (NURETH-16), Chicago, USA., 2015, p. 252.

[29] P. E. Angeli, M. A. Puscas, G. Fauchet, A. Cartalade, FVCA8 benchmark for the Stokes and Navier-Stokes equations with the TrioCFD code – benchmark session, in: Finite Volumes for Complex Applications VIII - Methods and Theoretical Aspects., 2017, pp. 181–202.

[30] D. Panunzio, M. A. Puscas, R. Lagrange, FSI-Vibrations of immersed cylinders. Simulations with the engineering open-source code TrioCFD. Test cases and experimental comparisons, arXiv 2101.11322 (2021).

[31] C. Fiorini, B. Després, M. A. Puscas, Sensitivity equation method for the navier-stokes equations applied to uncertainty propagation, International Journal for Numerical Methods in Fluids. (2020) 1–23.

[32] B. Van Leer, Towards the ultimate conservative difference scheme. V. A second-order sequel to Godunov's method, Journal of computational Physics. 32 (1979) 101–136.

[33] A. J. Chorin, Numerical solution of the Navier-Stokes equations, Mathematics of computation. 22 (1968) 745–762.

[34] R. Temam, Une méthode d'approximation de la solution des équations de Navier-Stokes, Bulletin de la Société Mathématique de France. 96 (1968) 115–152.

[35] S. Balay, S. Abhyankar, M. Adams, J. Brown, P. Brune, K. Buschelman, L. Dalcin, A. Dener, V. Eijkhout, W. Gropp, et al., Petsc users manual, Argonne National Laboratory Technical report (2019).

[36] C. Geuzaine, J.-F. Remacle, Gmsh: a three-dimensional finite element mesh generator with built-in pre- and post-processing facilities, International Journal for Numerical Methods in Engineering. 79 (2009) 1309–1331.